The solar rotation rate from inversion of the first GONG datasets

Thierry Corbard, Gabrielle Berthomieu, Janine Provost
Laboratoire G.-D.Cassini
Observatoire de la Côte d'Azur
Nice, France

Abstract

This poster gives some results obtained by inverting GONG datasets for the rotational splittings with a full 2D regularized least square method. This technique is based on a projection of the rotation on a tensorial product of B-splines, and could be very powerful to reach some fine information without increasing too much the number of variables.

A generalization to the 2D problem of the so-called L-curves is discussed and used as a guide for the choice of trade-off parameters.

The GONG months 4 to 8 datasets including both averaged (for degrees up to $l = 150$) and concatenated (for degrees lower than $l = 30$) spectra are inverted and discussed. The resolution of the inversion is studied using averaging kernels leading to an upper limit for the transition zone at the base of the convective zone.

The last available data from averaged spectra of GONG months 4 to 10 are inverted too. For this dataset, preliminary works on the introduction of a discontinuous basis of B-splines is presented.

References:

Christensen-Dalsgaard, J. & Berthomieu, G. 1991, in Solar Interior and Atmosphere, ed. A.N.Cox, W.C. Livingstone, & M. Matthews (Tuscon: Univ. of Arizone Press), 401.

T.Corbard, G. Berthomieu, G. Gonczi, J. Provost, P. Morel, 1995, Fourth Soho Workshop, Helioseismology, esa sp-376, 289-294.

Hansen, C., 1992, Numerical tools for analysis and solution of Fredholm integral equations of first kind, Inverse Problems 8: 849-872.

Ritzwoller M.H., Lavely E.M., 1991, ApJ 369, 557

Schou, J., Christensen-Dalsgaard, J. & Thompson, M.J. 1994, On comparing helioseismic two-dimmensional inversion methods, ApJ, 433: 389-416

Snodgrass, H.B., 1984, Solar phys., 94, 13.

Basic equations

An observable consequence of the solar rotation is that frequencies of solar oscillation modes (n,l,m) are splitted in a m multiplet. for low rotation the frequency shifts are given by:

$$\Delta\nu_{nlm} = \frac{\nu_{nlm} - \nu_{nl}}{m} = \int_{-1}^{1}\int_{0}^{1} K_{nlm}(r,\mu)\Omega(r,\mu)drd\mu \tag{1}$$

where ν_{nl} is the unperturbed mode frequency, $\Omega(r,\mu)$ is the unknown rotation rate versus depth and latitude, $\mu = \cos(\theta)$, θ is the colatitude and r the normalized solar radius. The kernels $K_{nlm}(r,\mu)$ depend on the model and the eigenfunctions of the mode which are assumed to be known exactly (e.g. Christensen-Dalsgaard & Berthomieu 1991).

We search for the unknown rotation as a linear combination of piecewise polynomials, projected on a tensorial product of B-spline basis (Corbard et al., 1995). We take into account the observational errors (with standard deviation σ_{nlm}) and a regularization term to avoid the large spurious variations of the solution induced by the ill-conditioned inversion problem. Thus we search coefficients that represent the projection of the rotation rate on the chosen B-splines basis by minimizing:

$$\sum_{nlm}\left(\frac{\int_{-1}^{1}\int_{0}^{1} K_{nlm}\Omega drd\mu - \Delta\nu_{nlm}}{\sigma_{nlm}}\right)^2 + \lambda_r T_r + \lambda_\mu T_\mu \tag{4}$$

$$T_r = \iint f_r(r,\mu)\left(\frac{\partial^i\Omega}{\partial r^i}\right)^2 drd\mu \quad T_\mu = \iint f_\mu(r,\mu)\left(\frac{\partial^j\Omega}{\partial \mu^j}\right)^2 drd\mu$$

The regularization parameters λ_r and λ_μ and functions f_r and f_μ are used to define the trade off between the resolution and the propagation of the input errors. We can choose any derivative of the rotation rate. This leads to different behavior of the rotation especially at locations where the observed modes are not enough to constrain the solution. For the results discussed here we choose $f_r = r$, $i = 2$ and $f_\mu = r^{-2j}$ with $j = 1, 2$.

The inversion depends on the number of piecewise polynomials, on the order of the spline functions and on the distribution of the break points of these polynomials. In what follows, the distribution of these points along the radius has been chosen according to the density of the turning points of the considered p-modes for a given dataset.

Averaging kernels

The inferred rotation $\tilde{\Omega}(r_0,\mu_0)$ at a point (r_0,μ_0) is obtained as a linear combination of the data $\Delta\nu_{nlm}$. Thus from Eq.(1) it follows that averaging kernels $\kappa(r_0,\mu_0,r,\mu)$, which are a linear combination of rotational kernels K_{nlm}, exist such that:

$$\tilde{\Omega}(r_0,\mu_0) = \iint \kappa(r_0,\mu_0,r,\mu)\ \Omega(r,\mu)drd\mu \tag{5}$$

The radial and latitudinal full widths at mid height (Δr and $r\Delta\theta$) of these kernels provide an estimation of the spatial resolution of the inversion at a point (r_0,μ_0). It increases with lower regularizing term, at the expense of larger errors on the solution.

Selected GONG datasets

We present the solutions obtained for two differents datasets. $l-\nu$ diagrams show the different modes concerned in each case.

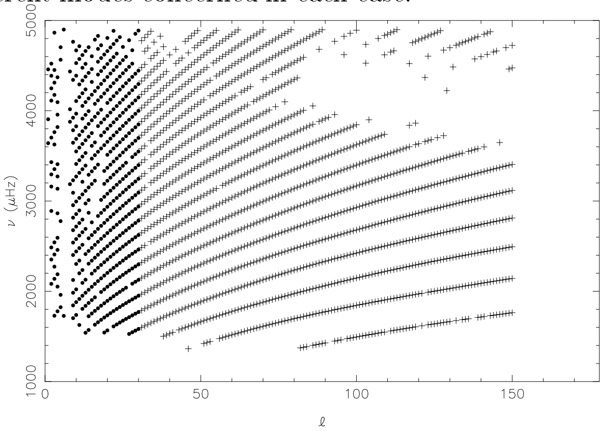

The first dataset (data I hereafter) is a combination of both concatened spectra of GONG months 4 to 8 for degrees lower than $l = 30$ and averaged spectra concerning GONG months 4 to 7 for degrees up to $l = 150$. It contains 1987 modes with $1200 < \nu_{nl} < 5000$ μHz. Splittings are given by their expansion on Legendre polynomials with coefficients up to a_9.

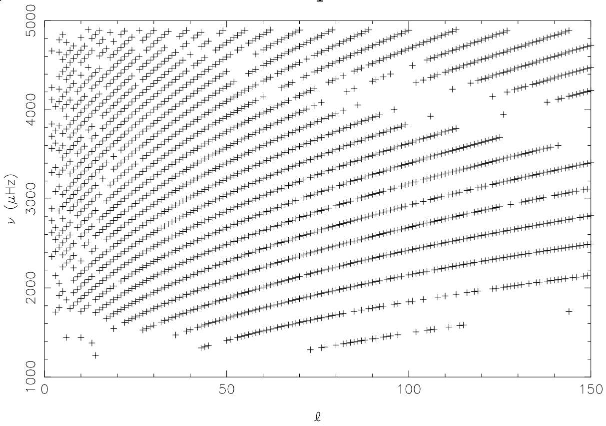

The second dataset (data II) has been obtained from averaged spectra of GONG months 4 to 10 for degrees $2 \leq l \leq 150$. It contains 2103 modes (n, l) $l \leq 150$ with with $1200 < \nu_{nl} < 5000$ μHz. Splittings are given by their expansion on orthogonal polynomials with coefficients up to a_9. The orthogonal polynomials are defined in Ritzwoller & Lavely (1991).

In both cases individual splittings and their corresponding errors have been calculated from their expansion on polynomials and inversions have been performed from these individual splittings.

L-curves: A guide for the choice of trade-off parameters ?

A guide for the choice of the trade-off parameters λ_r and λ_μ could be a generalization of the so called L-curves currently used in one dimensional problems (Hansen, 1992). The aim is to find parameters that minimize both the χ^2 value obtained for the fit of observed splittings (i.e. the first term in the sum Eq.(4)) and the two regularization terms T_r and T_μ.

One can plot the value of each part of the regularization term against the χ^2 value and this for different choices of λ_r and λ_μ. An interesting result is that in a log-log plot, for large values of the trade off parameters the χ^2 value gets large for little reduction of regularization terms and, in the opposite, for small values of lambdas the regularization terms get large for small reduction of the χ^2 value. Reasonable choices of trade-off parameters are therefore those in the vicinity of the corner of the L-curve.

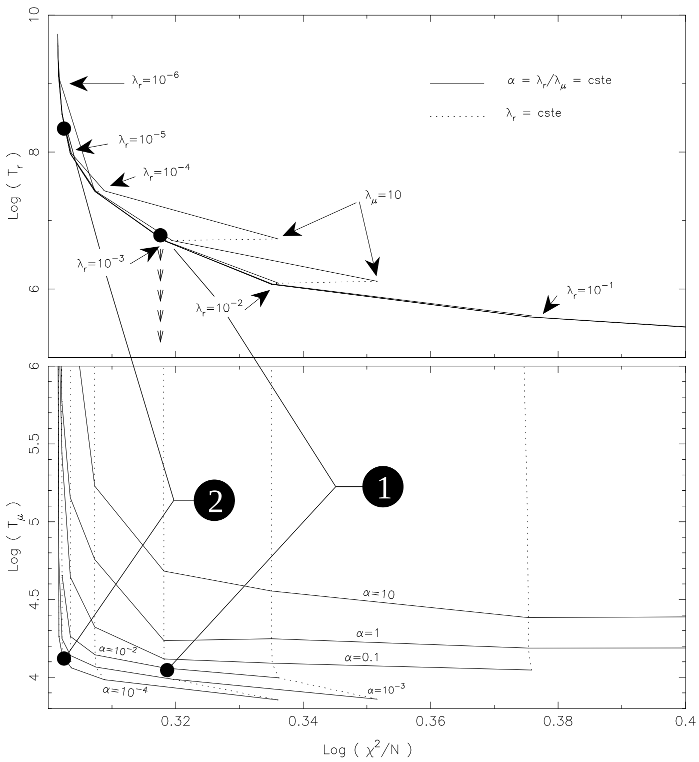

This figure shows an example of such L-curves obtained for dataset I and with second derivative ($i = 2$) in the regularization term in radius (T_r) and first derivative ($j = 1$) in T_μ.

The upper figure shows the logarithm of the value of the regularization term T_r against $\log(\chi^2/N)$ where N is the total number of splittings, this for different values of λ_r and λ_μ. One can see that all the points on this figure which are labeled by the same λ_r but different λ_μ have the same location except for very large values of λ_μ (i.e. $\lambda_\mu > 1$) . Thus it appears that the two terms (χ^2 and T_r) **do not depend on the value of λ_μ for a large domain of variation of this parameter ($\lambda_\mu \leq 1$).**

The full curves join points with the same ratio $\alpha = \frac{\lambda_r}{\lambda_\mu}$. According to the previous discussion, on the upper figure all these curves reduce to only one if we do not look at solutions obtained with $\lambda_\mu > 1$ that are too much regularized.

On the lower figure the value of the logarithm of the regularization term T_μ is plotted against $\log(\chi^2/N)$ for six values of the ratio α. As α decreases the position of the L-curve becomes lower showing that for a given value of λ_r, the λ_μ value must be as large as possible (always with the limitation $\lambda_\mu \leq 1$) if one wants to reduce the value of the regularization term in latitude.

According to these two figures, a choice like point 1 on the figure ($\lambda_\mathbf{r} = \mathbf{10^{-3}}$, $\lambda_\mu = 10^{-1}$, i.e. $\alpha = \mathbf{10^{-2}}$) tends to minimize both the χ^2 value and the two regularization terms.

When a regularization term in latitude T_μ is chosen with second derivative ($j = 2$), the corresponding plots have similar behaviors but the domain of variation for λ_μ, for which χ^2 and T_r depend only on λ_r, is smaller ($\lambda_\mu \leq 10^{-1}$).

L-curves reveal themself as being an useful tool to study the variation and mutual dependencies of each term in Eq.(4) for different choices of trade-off parameters and functions f_r and f_μ. Nevertheless other methods for the optimal choice of trade-off parameters are possible. In particular, for a local estimation of the quality of the solution, we must have a look at the balance between the effect of propagating input errors and the resolution reached at a target location ($\mathbf{r_0}, \mu_\mathbf{0}$).

A solution with dataset I and
L-curves based choice for the trade-off parameters

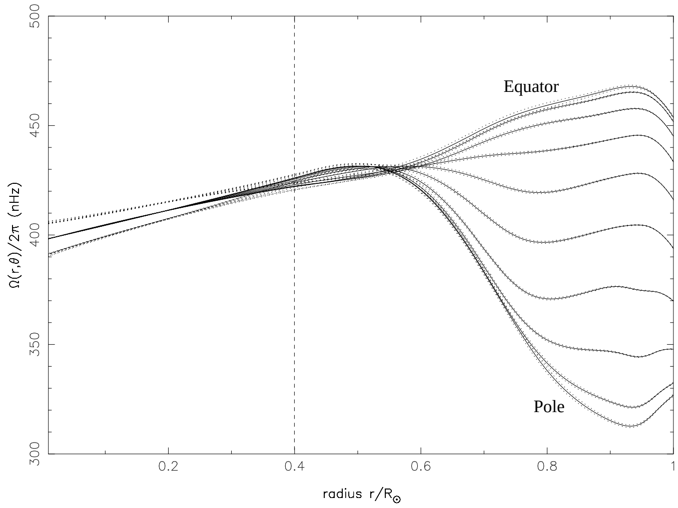

The inferred rotation rate is shown as a function of radius for ten latitudes from the equator up to the pole ($\theta = 90°, 80°, .., 0°$). This solution is very smooth and has no latitudinal dependence below 0.6 solar radius.

Below $0.4R_{\odot}$ the solution is not reliable because of the lack of modes able to describe these depths leading to averaging kernels that are large, not well localized and that consist in several peaks. The latitudinal independence found for these depths results essentially from the choice of $j = 1$ in the regularization term T_{μ}. This choice could be judicious for an attempt to sound the very deep interior from such global inversion, without searching for a description of a latitudinal dependence in the core that should require very low errors in data. Nevertheless, our current investigations and the averaging kernels that we obtained do not allow us to draw an inference from the solution obtained below $0.4R_{\odot}$.

In the whole convection zone the rotation rate presents the same latitudinal variation as at the surface with a positive gradient just beneath the surface for latitude from the equator up to 50°. The transition to a latitudinal independent rotation in the radiative zone occurs between 0.8 and 0.6 solar radius for latitude up to 70°.

Dotted curves represent the 1σ errors on the solution which are the result of propagating input errors on the splittings through the inversion. In this inversion these errors are very low because the regularization is very strong. In fact these errors represent the difference between the inferred rotation and the true rotation rate convolved with the averaging kernels as in Eq.(5).(see e.g. Schou et al 1994). A look at these kernels is needed to qualify the resolution of the inversion.

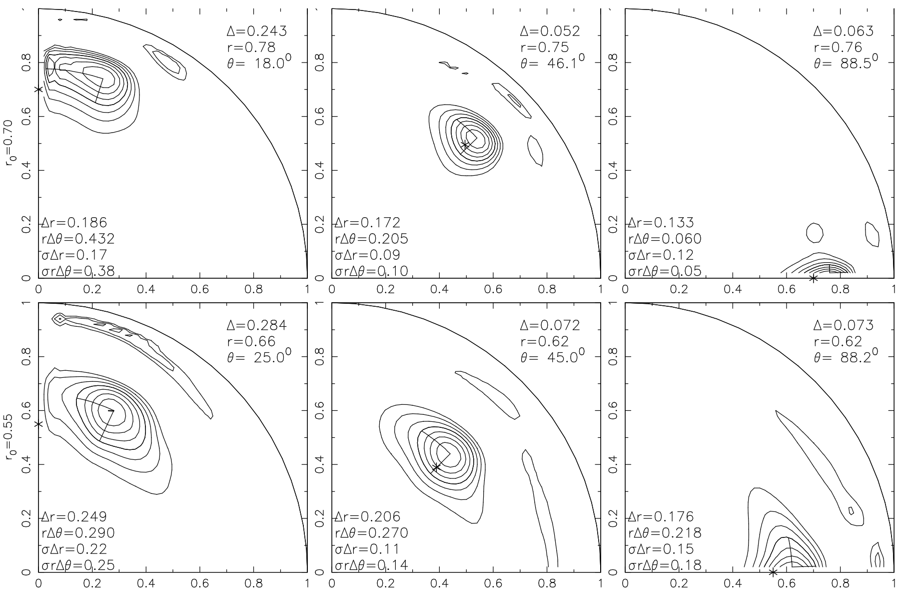

These figures show contour plots of the averaging kernels at solar pole, mid latitude and equator for $r_0 = 0.55,\ 0.70\ R_\odot$. Δ is the geometrical distance between position (r, θ) of the maximum value of the averaging kernel and the point (r_0, θ_0) shown as a star on figures. This quantity is very high for averaging kernels calculated near the pole ($\Delta = 0.25$), showing that for these latitudes we are not able to obtained well peaked kernels and inferred the solution is not reliable.

At $0.55R_\odot$ the estimated rotation rate is latitudinal independent. Nevertheless the latitudinal resolution at $0.55R_\odot$ is very low ($\Delta\theta \simeq 30^\circ$ at mid latitude) and could produce a smoothing effect on a latitudinal variation if any exists.

The radial resolution at the base of the convection zone ($r = 0.7R_\odot$) is around $\Delta r = 0.17R_\odot$ at mid latitude and is almost as large as the transition observed on the solution ($0.2R_\odot$). Thus if the transition is sharper this inversion doesn't enable to resolve it. Inversions with less regularization have been performed to study this transition zone.

How sharp is the transition zone ?
Results of inversions with less regularization

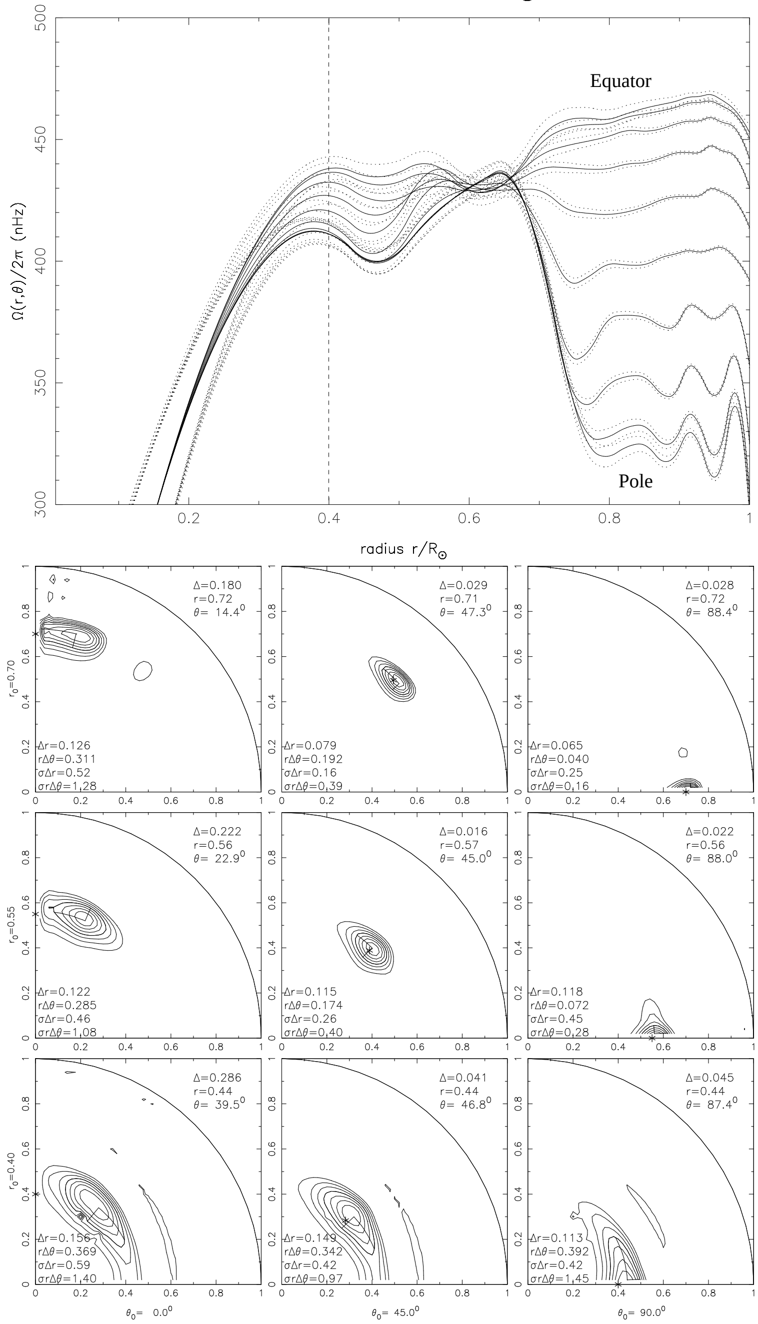

These figures show the inferred rotation rate with $\lambda_r = 5.10^{-6}$, $i = 2$ and $\lambda_\mu = 10^{-2}$, $j = 1$ and the corresponding averaging kernels for $r_0 = 0.4, 0.55, 0.70 R_\odot$ and $\theta_0 = 0°, 45°, 90°$. This choice of trade-off parameters, (shown as the point 2 on L-curves figure) tends to minimize the χ^2 value rather than the two regularization terms. This leads to a solution with some oscillations especially in zones near the solar pole where the solution is not well constrained by the data.

This inferred rotation rate has a sharper transition zone than the previous one (about $0.10 R_\odot$) and the averaging kernels at this location ($r = 0.7 R_\odot$) are better peaked with an increasing radial resolution ($\Delta r = 0.08 R_\odot$ at mid latitude). Inversion performed with lower regularization doesn't enable to produce better radial resolution and increase the effect of input errors, leading to an increasing product $\sigma \Delta r$. Thus, this inversion is the one that gives the best radial resolution at this target location without increasing to much the effect of input errors. **The fact that the width of the transition zone decreases when the resolution increases allows us to say that the transition occurs in a zone between 0.66 and 0.76 solar radius but it might be sharper than this.**

At $0.55\mathbf{R}_\odot$ averaging kernels at $0°$, $45°$ and $90°$ are, for this inversion, sufficiently well localized in latitude so that the latitudinal independence of the inferred rotation rate at this depth can be considered as real.

At 0.4 $R_\odot$ the large extent in latitude of the averaging kernels should produce a smoothing effect i.e. almost the same averaged rotation rate for all latitudes. Nevertheless, the solution shows again a latitudinal dependence between 0.55 and 0.35 $R_\odot$. This might argues in favor of the existance of a variation with the latitude at these depths but we are still studying how to read our results there: some contributions in averaging kernels generated by a lack of cancelation of rotational kernels near the surface are suspected and may explain this behavior of the inferred rotation rate in this kind of inversion with low regularization. Moreover this latitudinal dependence below $0.55 R_\odot$ is of lower importance with dataset II.

Results from dataset II and Preliminary works on the introduction of a discontinuous Basis of B-splines

The solution obtained from dataset II is shown on the upper transparency for radius above $0.4R_\odot$. The choice of trade-off parameters correspond to the point 2 on the L-curves figure. The inferred rotation rate is in good agreement with the previous one for latitudes below 60° and is less oscillating near the pole. As the observed modes and the trade-off parameters are the same as for dataset I, we can think that these zones are now better constrained by the data. Nevertheless we can not exclude that the regularization acts not exactly by the same way on the two datasets so that the regularization could be more important with dataset II.

The possibility of introducing a discontinuous basis of B-splines might give a test of the reliability of the inferred rotation rate at a target radius. The idea is to allow the rotation to be discontinuous at a given depth and to look, after inversion, if the inferred rotation is discontinuous at this location or not. Solutions that are physically realistic should be continuous at each point but in zones where the solution is not well constrained such inversion could produce different values for the rotation rate on the right and on the left of the break point. Our preliminary results show that the gap between the right and left values is low where the solution is thought to be well constrained by the data and larger elsewhere.

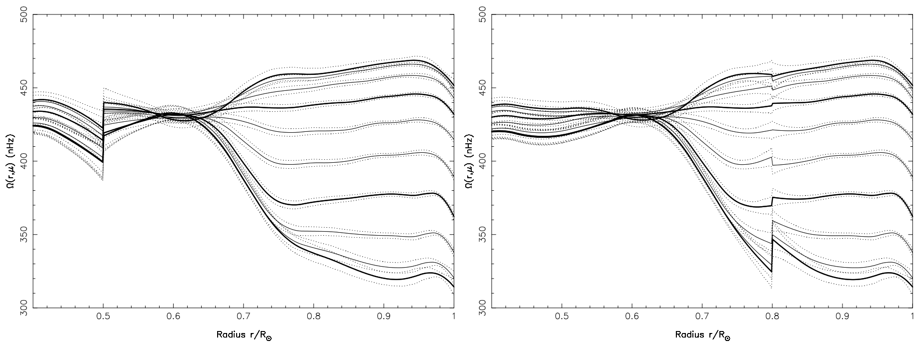

These figures show examples of solutions obtained when we allow it to be discontinuous at $0.8R_\odot$ and $0.5R_\odot$. At $0.8R_\odot$ the solution remains continuous at the equator and the gap increases with the latitude up to 40 nHz at the pole. With a discontinuous basis at $0.5R_\odot$, the gap is around 40 nHz even at the equator. Other results show that the gap increases again in the deep interior. In all cases the value at the middle of the gap is equal to the value of the rotation rate that we obtain without introducing any discontinuous basis. Therefore this tool should provide an alternative way to estimate the error on the solution and to show how the inversion is stable at a target location.

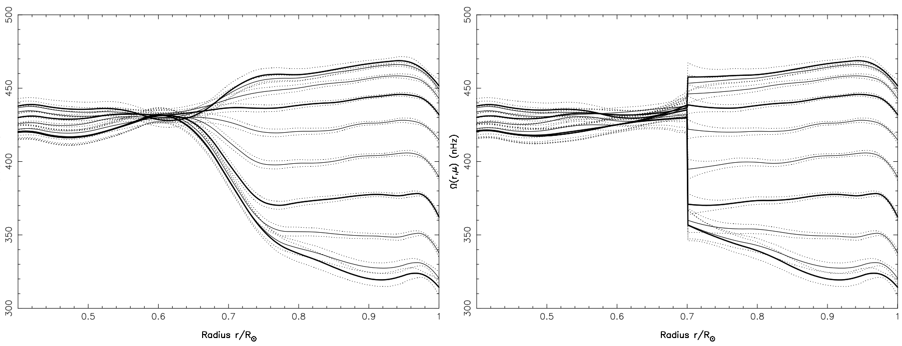

We are also studying the possibility of using similar tools to estimate the thickness of the transition zone. An example is given on the lower transparency that shows the solution obtained when we allow the rotation to be discontinuous at the base of the convection zone ($0.7R_\odot$).

The χ^2 value obtained for this solution and the resolutions are almost the same than with the standard basis indicating that data are compatible with a very sharp transition zone.

Averaging kernels obtained at the equator and $0.69R_\odot$ are shown for the solutions obtained with and without setting a discontinuous basis at $0.7R_\odot$ (shown on the two transparencies). Although, without discontinuous basis the averaging kernel was equally distributed around $0.7R_\odot$, with a discontinuous basis the major part of the kernel is below $0.7R_\odot$. By this way the value of the rotation rate obtained at $0.69R_\odot$ is less influenced by the true rotation above $0.7R_\odot$ and this could explain its lower value. This may argue in favor of a solid rotation up to $0.69R_\odot$ but this conclusion would have been more reliable if the averaging kernel had strictly no part above $0.70R_\odot$. Furthermore the new averaging kernel is more oscillating between 0.72 and $0.9R_\odot$ so that its interpretation is harder. A symmetrical example is shown by the averaging kernels calculated at the equator and $0.71R_\odot$ with and without allowing the rotation to be discontinuous at $0.7R_\odot$. This could explain by similar way the higher value obtained just above $0.7R_\odot$ when we perform the inversion with a discontinuous basis.

This work is very preliminary and we think that numerical experiments on the reconstruction of some arbitrary given test rotation rates should be useful to calibrate the effect of introducing a discontinuous basis.

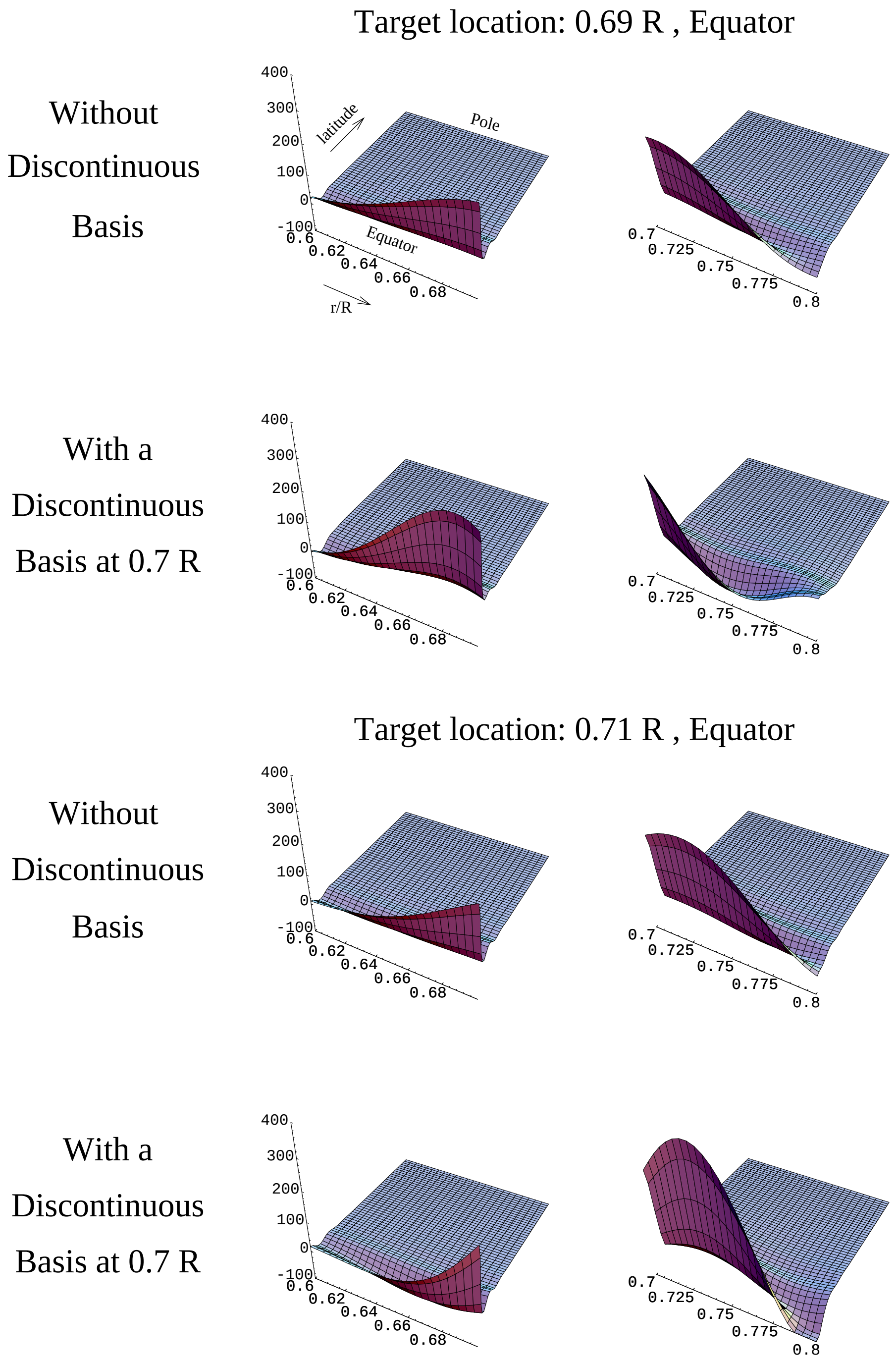
Target location: 0.69 R , Equator
Without Discontinuous Basis
With a Discontinuous Basis at 0.7 R
Target location: 0.71 R , Equator
Without Discontinuous Basis
With a Discontinuous Basis at 0.7 R
latitude
Pole
Equator
r/R
400
300
200
100
0
-100
0.6
0.62
0.64
0.66
0.68
0.7
0.725
0.75
0.775
0.8